Perturbation induced by EDTA on HDO, Br- and EuIII diffusion in a large-scale clay rock sample

R.V.H. Dagnelie, P. Arnoux, J. Radwan, D. Lebeau, P. Nerfie, C. Beaucaire

HAL Id: hal-04240835

https://hal.science/hal-04240835

Submitted on 13 Oct 2023

Perturbation induced by EDTA on HDO, Br- and Eu^{III} diffusion in a large-scale clay rock sample.

R. V. H. Dagnelie[a,*], P. Arnoux[a],

J. Radwan[a], D. Lebeau[b], P. Nerfie[a] C. Beaucaire[a]

[a] CEA, DEN, DANS, DPC, Laboratory of Radionuclides Migration Measurements and Modelling,

F-91191 Gif-sur-Yvette, France.

[b] CEA, DEN, DANS, DPC, Laboratory of Radiolysis and Organic Matter,

F-91191 Gif-sur-Yvette, France.

* Corresponding author: Romain V.H. Dagnelie, Tel: +33 1 69 08 50 41; fax: +33 1 69 08 32 42.

Email address: romain.dagnelie@cea.fr

Highlights

A large-scale clay rock sample was perturbed by a 10 mM EDTA plume for 450 days.

Dissolution of carbonates (fast) and iron-rich phases (slow) was monitored.

Perturbation modified speciation equilibrium but had a limited effect on transport.

Transport parameters of HDO, Br, EDTA, Eu, including anisotropy were quantified.

EDTA and Eu-EDTA complexes displayed a strong desorption hysteresis.

Abstract

Clay rocks are widely studied in the context of waste landfill leachates or as geological barriers for nuclear waste management. The release of organic co-contaminants by wastes may alter clay rocks, depending on the ratio between the volume of wastes and the mass of rock. In this work, a 10 mM EDTA plume was injected in a large-scale clay rock sample with a low V/m ratio ($<<$ 1.0 L kg^{-1}) close to environmental conditions. The chemical perturbation was monitored for 450 days, as well as its effect on HDO, Br$^-$, and Eu^{III} diffusion. Alteration of carbonates and iron-rich phases was evidenced in addition to the decrease of tracer concentration. Negatively charged complexes of EDTA and Eu are slightly adsorbed on minerals surface and display a desorption hysteresis. Transport parameters including diffusion anisotropy of HDO, Br, and EDTA complexes are estimated. Results are discussed with emphasis on determination of the mechanisms governing such perturbation and the corresponding transitory state.

Graphical Abstract:
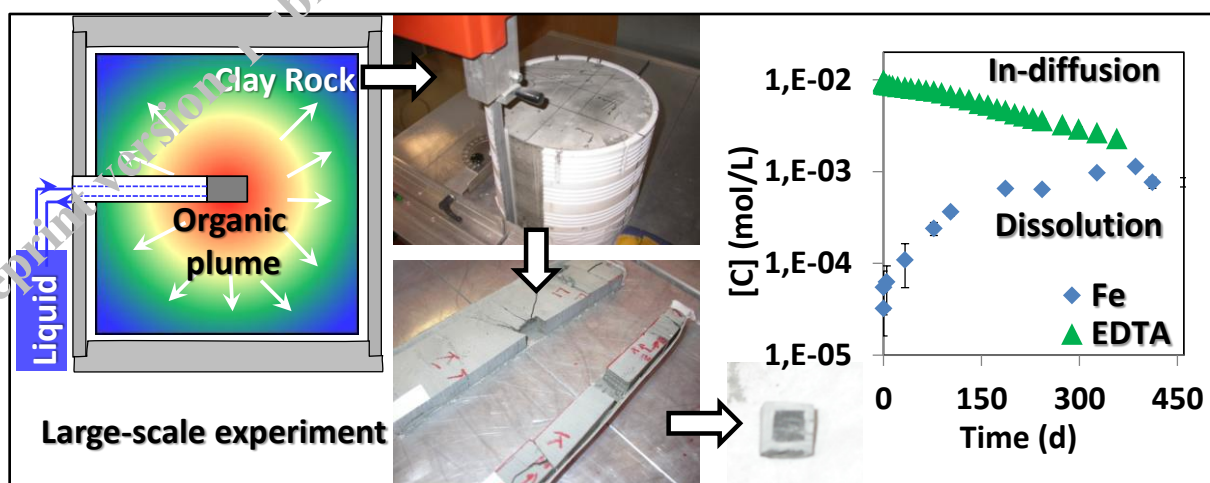
Keywords: Diffusion, Sorption, Clay, EDTA, anisotropy, Large-scale

1. Introduction

The fate of cations in the environment is of interest in various fields such as landsite pollution by toxic chemicals, extraction of ore, impact of mining industry and nuclear waste management. A mechanism that is known to largely affect cations behaviour is the interaction with organic matter (Harter and Naidu, 1995; Bryan et al., 2012). One can classify organics in two families. Natural organic matter (NOM) is present in raw materials such as peat-bog, sedimentary rocks or dissolved in aquifers. Anthropogenic organic matter (AOM) is released by dissolution of wastes and engineered materials. Numerous studies deal with complexation capacity of NOM and effects of humic substances on radionuclides transport (Bryan et al., 2012; Reiller, 2012). Phenomenological models are available, such as the one provided by Maes et al. (2011) on diffusion of radionuclides linked to NOM in Boom Clay, or by Alonso et al. (2011) on colloids diffusion in various clay rocks. One may also find numerous studies on adsorption of dissolved organic matter in various soils (Guggenberger and Kaiser, 2003; Pignatello, 1999). However, reactivity and alteration of materials by AOM is less investigated even if it is known to be crucial in some cases, for example in mineral weathering (Drever and Stillings, 1997). This work deals with dissolved AOM, also called co-contaminants, and their disrupting effect on a sedimentary clay rock and its containment properties.

Clay rocks have numerous applications as geological barriers: for treatment of industrial effluents and waste landfill leachates (Churchman et al., 2006), or nuclear waste disposal (Lee and Tank, 1985). We chose to study a Callovo-Oxfordian (COx) clay rock, which is investigated by the French radioactive waste management agency (ANDRA, Gaucher et al., 2004) in the context of the underground retrievable nuclear waste repository project (Cigéo). Numerous data are available on this clay rock, including diffusion of cations (Melkior et al., 2007), diffusion of anions (Descostes et al., 2008; Savoye et al., 2012a), diffusion of organic co-contaminants (Dagnelie et al., 2014) and organic macromolecules (Durce et al., 2014). Most of these studies use standard diffusion cells at a centimetric scale. Only few "large-scale" experiments were performed in order to validate diffusion parameters of HTO, Cl^-, Na^+ and Sr^{2+} (Cormenzana et al. 2008; Samper et al. 2008; Garcia-Guttiérez et al., 2008)

and also with HDO, $H_2^{18}O$, Br^-, and Cs^+ through an Opalinus clay sample (Savoye et al., 2012b). Moreover, in situ experiments were performed on metric scale in Bure underground research laboratory (Poinssot and Geckeis, 2012) with various anionic and cationic tracers such as HTO, $^{22}Na^+$, $^{125}I^-$, $^{85}Sr^{2+}$ and $^{134}Cs^+$. Martens et al. (2009) also presented in situ diffusion of ^{14}C-labelled NOM in Boom clay at a metric scale and Gimmi et al. (2014) gathered results of in situ experiments with various tracers in Opalinus clay. For most of these studies, the transport parameters obtained at various scales are mutually consistent. This confirms that adsorption/diffusion processes are rather independent of the ratio between the volume of the liquid source and the mass of solid (V/m) in the case of a steady state between both phases. Thus, similar results are expected with batch experiments (V/m ~ 1-500 L kg^{-1}), diffusion cells (V/m ~ 1-100 L kg^{-1}), large-scale laboratory experiments (V/m ~ 10^{-3}-10^{-2} L kg^{-1}) or in situ experiments (V<<m).

In the case of nuclear waste storage or pollution by hazardous wastes, high concentration of co-contaminants can be released, inducing a chemical or physical perturbation of the system. For example, wastes may release nitrate or sulfate plumes, generate gases such as N_2/CO_2 by degradation or H_2 by radiolysis, induce heating of the material, or release organic molecules leading to degradation or dissolution (enhanced by oxidation or bacterial activity). A transitory state is expected during such perturbation and its duration and spatial spreading depend on the ratio between the source term and the mass of rock (V/m). This work focuses on the perturbation induced by an organic plume in a large-scale clay rock sample with low V/m ratio representative of in situ conditions. The organic complexing agent chosen in this study is ethylendiaminetetraacetate (EDTA). EDTA is used in various fields such as decontamination processes of soils and wastewater treatment (Nagy et al., 1999; Pociecha and Lestan, 2012), industrial processes such as pulp and paper processes (Pokhrel et al., 2004). Its mobility and high complexing capacity make it hindering in term of pollutants migration through the biosphere. Thus, impact of EDTA is investigated in various research areas, such as radionuclide's mobility in soils/groundwater system (Seliman et al. 2010), natural sand (Reinoso et al., 2012) and retention of trace metals in clays (Darban et al. 2000). The following study presents the perturbation of a large-scale COx clay rock sample by a 10 mM EDTA plume. The aim is to

characterize transport parameters of various tracers (cationic Eu[III], anionic Br^{-}, and neutral HDO) in the perturbed rock. Another aim is to determine the spatial spreading and duration of such perturbation with a low V/m ratio, representative of in situ conditions. Analysis and modelling of the results are performed with emphasis on the determination of relevant mechanisms in addition to the diffusive transport.

2. **Materials and Methods**

2.1 Clay rock characterization and preparation

Experiments were carried out on a single core sample (DIR1004, EST27325) collected at a depth of 490 m below ground level in the DIR1004 borehole in the ANDRA underground laboratory (Bure, France). Sample dimensions are 290 mm of diameter and 250 mm of length. Clay rock sample was protected from oxidation and mechanical alteration by placement in a Teflon cylinder and in anoxic aluminum containers under N_2. Once in the laboratory, the rock with the Teflon shell was placed in a stainless steel cylindrical cell (Figure 1). One horizontal hole of 21 mm of diameter was drilled and filled with a stainless steel injection chamber. The extremity of the chamber includes a PEEK cylinder of 21 mm of diameter and 40 mm of length corresponding to the solid solution interface.

Figure 1. Top : Picture of the clay rock in its stainless steel cell. Middle: Scheme of the experimental setup. Bottom: Mesh and geometry of the solid profiles.

The initial saturation degree of the rock was evaluated to 85 %, by weight measurement after heating at 105 °C. A first step of rehydration of the clay rock sample was performed over almost 600 days to reach clay saturation close to the injection chamber, in order to ensure a mainly diffusive transport. The
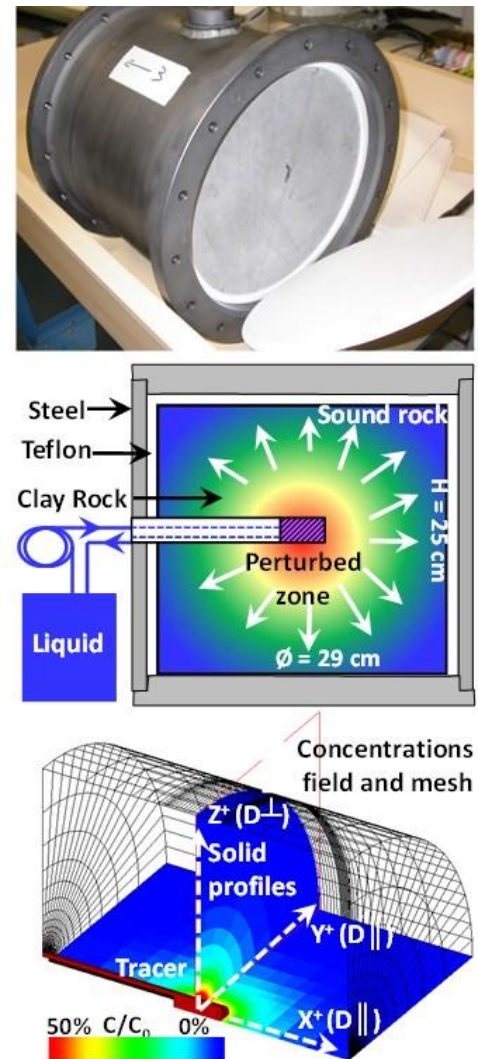
composition of the synthetic porewater used during the hydration step is given in table 1. Concentration of major ions was measured by ion-chromatography (DX-500 and DX-120 from DIONEX with AS14 and CS17 columns). Alkalinity was measured by UV-Vis spectrophotometry with a Cary-500 device from Agilent Technologies and titration method with formic acid and bromophenol blue (Sarazin et al., 1999). High purity salts were used to prepare the injection solution: disodium Na_2H_2EDTA (Fluka #03679, purity > 99 %), $EuCl_3$ (Alfa Aesar, REacton®, purity > 99.99%). The composition of the injection solution was calculated according to the equilibrium at the end of hydration step. Then Na_4EDTA and $EuCl_3$ were added at concentrations gathered in table 1. The pH of the injection solution was adjusted to 7.1 ± 0.1 with concentrated NaOH or HCl standard solutions. In order to obtain transport parameters, one requires the concentration in the liquid as a function of time as well as the spatial distribution of tracers in the rock at the end of the experiment. These data were obtained using analytical methods described in sections 2.2 and 2.3 respectively.

Ions $(10^{-3} mol\ L^{-1})$	$[Na^+]$	$[K^+]$	$[Ca^{2+}]$	$[Mg^{2+}]$	**$[Eu^{3+}]$**	$[Cl^-]$	Alk.	$[SO_4^{2-}]$	**[EDTA]**
Hydration	49.5	1.0	4.9	3.4		49.3	2.7	7.5	
Equilibrium	56.2	1.02	6.4	6.8		53.0	6.6	8.5	
Injection t = 0$^+$	86.1	1.0	8.0	5.8	**0.21 ± 0.006**	70.2	6.5	8.7	**9.30 ± 0.3**
t = 404 d	**[HDO] = 1893 ± 80 ppm ; [Na$^+$Br$^-$] = 2.81 ± 0.07 10^{-2} mol L^{-1}**								

Table 1. Composition of the synthetic solution used for hydration step and

equilibrium water measured after one year and used for injection.

Values written in bold represent tracers injected at t= 0 (Eu, EDTA) and t= 404 d (HDO, Br).

2.2 Diffusion experiments and liquid monitoring

The diffusion step started when 140 mL of the injection solution was connected to the circulation system. The initial concentrations were $9.3\ 10^{-3}$ mol L^{-1} for EDTA and $2.1\ 10^{-4}$ mol L^{-1} for Eu^{III}. Aliquots of the liquid were periodically withdrawn using a sampling loop with a volume of

433±2 μL. Sampling loop was renewed with the synthetic solution without tracers. A dilution in 2% HNO₃ was performed for further measurement of Eu by Inductively Coupled Plasma Mass Spectrometry (ICP-MS). EDTA was measured by UV-Vis titration method with iron described by Uzumasa et al. (1956). After 404 days, 1.2 mL of solution containing HDO and NaBr was injected in the system. The initial concentrations for HDO and bromide were 1893 ppm (i.e. 11153 ‰ vs SMOW) and $2.81 \ 10^{-2} \ mol \ L^{-1}$ respectively. HDO and Br⁻ tracers were then monitored during 56 days using the sampling loop but without renewing the sampled aliquots. Concentration of HDO were measured with a deuterium-analyzer (CRDS, Los Gatos Research, USA) and bromide analyzed by ion-chromatography.

Additional measurements were performed in order to quantify the chemical perturbation of the equilibrium in solution. The concentration of major ions was measured using DX-500 and DX-120 ion chromatography systems (Dionex Co, UK). These systems were equipped with IonPac® AS17-AG17 and CS12A-CG12A columns for measurements of anions and cations respectively. The speciation of EDTA in solution was determined by means of Electro Spray Ionization Mass Spectrometry (ESI-MS, Nogueira et al., 2009) on a LCT Premier equipped with an Electro-Spray source (Micromass, Manchester, UK) in negative W mode. The release of iron from the rock was also monitored in the liquid samples. The concentration of iron in solution was measured by atomic absorption using an AA240FS device from Varian since UV-Vis methods were found to be difficult in presence of variable amount of EDTA.

2.3 Characterization of solid profiles

460 days after the injection, the liquid system was disconnected from the clay rock. The rock sample was extracted from the cell using a steel lid and a hydraulic jack (RC104 from ENERPAC, F = 101 kN at 700 bars). Cutting was performed using a bandsaw to obtain several solid profiles centered on the injection chamber and along the 5 axis available (X⁺, Y⁺, Y⁻, Z⁺, Z⁻). The size of each rock profile was ~15×15 mm², 115 mm along Z axis and 135 mm along XY axes. Each solid profile was finally cut into 12 to 16 samples using a wire saw, with lengths varying from 4 mm close to the injection chamber up to 20 mm. Rock samples were placed in centrifugation tubes and weighed.

Milli-Q® water was added with a solid liquid ratio of 1 g mL^{-1}. Samples of the X$^+$, Y$^+$, Y$^-$, Z$^+$, and Z$^-$ profiles were agitated for leaching during one week. Tubes were centrifuged at 50 000 g during 1 hour and the supernatant was removed for analysis of HDO, Br$^-$, Eu^{3+} and EDTA. A duplicate of the Y$^-$ profile was used to measure the total concentration of Eu^{III}. For that purpose, samples were crushed and 200 mg were weighed in a Teflon tube, completed by 10 mL of 69% HNO$_3$, 5 mL of 40% HF and 45 mL of Milli-Q® water. Samples were mineralized by heating 2 hours inside a micro-wave (DAK-100 from Speedwave) under a pressure of 100 bars and a temperature of 300 °C. The total amount of europium was then quantified by ICP-MS.

2.4 Modelling and transport parameters

The transport of the species is supposed to be mainly diffusive. The analysis of the results is based on Fick's second law for 3-dimensional reactive transport (Cranck, 1975):

$$\frac{\partial C}{\partial t} = \frac{D_e}{\varepsilon_a + (1-\varepsilon_a)\rho K_d}\nabla^2 C = \frac{D_e}{R \times \varepsilon_a}\nabla^2 C = \frac{D_e}{\alpha}\nabla^2 C \tag{1}$$

where C is the concentration (mol m^{-3}); t, the time (s); D_e, the effective diffusion coefficient (m^2 s^{-1}); ε_a, the diffusion-accessible porosity; ρ, the grain density ($\sim$2700 kg m^{-3}); K_d, the sorption distribution ratio (m^3 kg^{-1}) and α the rock capacity factor. The retardation factor is defined as R=α/ε_a=1+ρKd(1-ε_a)/ε_a. D_e is the diffusion coefficient along the vertical axis, Z, which is perpendicular to the clay rock bedding. The effective diffusion along X and Y axes is considered to be D_e (X) = D_e (Y) = a × D_e (Z), with "a", called diffusion anisotropy. The adjustment of experimental results is performed using three variable parameters: the effective diffusion, D_e, the rock capacity factor, α, and the diffusion anisotropy, a. The adsorption distribution ratio, K_d (L kg^{-1}), for adsorbent species is defined by

$$K_d = \frac{C_{ads.}}{C_{liquid}} \tag{2}$$

where C_{ads} is the concentration of adsorbed species (mol kg^{-1}) and C_{liquid} the concentration in solution or at equilibrium with the clay (mol L^{-1}). Adsorption equilibrium is expected before and after the leaching of the samples. The quantity of A after leaching is calculated by the initial quantity in the sample and the quantity of A within dilution water, leading to equation (3):

$$[A]_{leached}^{experimental} = \frac{[A]_{poral}^{calculated}(\frac{m}{\rho} \times \varepsilon_a + m \times K_d) + [A]_{mQ} \times V_{mQ}}{(\frac{m}{\rho} \times \varepsilon_a + m \times K_d + V_{mQ})} \tag{3}$$

$[A]_{mQ}$ is equal to zero for EDTA, Eu and Br⁻, and was measured for deuterium, $[HDO]_{mQ} = 149.5 \pm 0.5$ ppm. Equation (3) illustrates the relationship between analytical results($[A]_{leached}$) and data calculated by the simulation ($[A]_{poral}$).

The solution of equation (1) is calculated at each sampling time numerically using the ALLIANCES platform (Montarnal et al., 2007). The mesh used for calculation is presented in figure 1 and consists of 25,000 elements. It includes a quarter of the rock sample which displays two planes of symmetry (OXY and OXZ). Thus the modelling of Y^+ (Z_+) profile is sufficient to adjust both Y^+ (Z_+) and Y^- (Z_-) results which are symmetrical duplicates. The boundary conditions impose a flux equal to zero outside the mesh. The initial conditions are $[A]^{solution}(t=0) = C_0$, $[A]^{solid}(t=0) = 149.5$ ppm for HDO and $[A]^{solid}(t=0) = 0$ for other species.

The concentration modeled in the liquid as a function of time is compared to experimental monitoring. The concentrations of leached solid samples are compared to results calculated for the cutting time at the same coordinates (XYZ). For each species, parameters (De, α, a) are adjusted by a minimization algorithm. The minimization criterion is calculated by integrating differences between all experimental and modelled data. A ponderation factor is used for each data and is inversely proportional to the uncertainty. Besides, the same statistical weight is given to the adjustment of the liquid monitoring and of all the solid profiles.

3. Results

3.1 Liquid monitoring

The concentration of tracers is given in the figure 2. The initial concentration of HDO is high compared to the concentration measured in sound clay rock samples considered as $[HDO]_{COx}$ ~ $[HDO]_{mQ} = 149.5 \pm 0.5$ ppm. HDO concentration decreases by 50 % within 56 days. The decrease of Br- is slower, at around 20 % after 56 days, indicating a low apparent accessible porosity and effective diffusion coefficient due to anionic exclusion. The adjustment of transport parameters will be described in the section 4: modelling.

The very slow decrease of Eu^{III} in solution which usually displays high adsorption on clay rock ($K_d(Eu^{III}/COx) \sim 2.2 \times 10^4$ L kg^{-1} (Andra, 2014)) is due to its complexation by EDTA. The [Eu-EDTA]$^-$ complex is then expected to display a low adsorption as well as a low effective diffusion coefficient. In contrast, a sharp decrease of EDTA is observed and likely originates from adsorption processes and/or reactivity with clay rock.

Figure 3 shows the evolution of ions concentration in the injection chamber during the experiment. The strongest evolution is observed within the first 300 days. The concentrations of Mg^{2+} and especially Ca^{2+} present the fastest increase within 80 days, suggesting a modification of the equilibrium between solid phases and solution with EDTA. Speciation calculation using PhreeqC (Parkhurst, 1995) gives the following saturation indexes: $s^C = -1.1$ and $s^D = -0.8$ for calcite and dolomite respectively at $t = 0$ and $s^C = 0.4$ and $s^D = 1.0$ at $t = 100$ days. This result is in agreement with the hypothesis of a fast equilibration between the fluid and carbonate minerals. Calcite and dolomite are initially under saturation because of the complexation of Ca^{2+} and Mg^{2+} by EDTA. Then dissolution of Ca^{2+} occurs until the equilibrium, which is probably imposed by calcite, is reached. The other ions display a slow and constant increase during 300 days (by 64 %, 133 %, 60 %, and 39 % for Ca^{2+}, Mg^{2+}, SO_4^{2-} and K^+ respectively). The further and linear increase in Mg^{2+} and K^+ concentrations corresponds more likely to a slow adsorption / desorption rearrangement induced by the spread of the Na_4EDTA plume. Na^+ diffuses from the injection chamber toward the rock and sorbs on clay minerals. The desorption of other cations leads to a retro-diffusion toward the injection chamber and the slow increase of concentration in solution.

EDTA speciation was measured by ESI-MS experiments. Three main signals were observed for EDTA species, at m/z = 335, 344 and 351, corresponding to [MgNaEDTA]$^-$, [Fe^{III}EDTA]$^-$ and [CaNaEDTA]$^-$ respectively. The S^{351}, S^{344} and S^{335} signals were corrected using S^{97} as an internal standard (m/z(HSO$_4^-$)=97). The corrected signals for other species, S*, are then calculated from the raw signal (S) using the following equation: $S^*(t)=S(t)/S^{97}(t)\times[SO_4^{2-}](t)/[SO_4^{2-}]_0$. The sum of the corrected signals for the three EDTA species observed, $S^{TOT}=S^{*351}+S^{*344}+S^{*335}$, is given in figure 2 and compared to the total concentration of EDTA. A good agreement is observed between ESI-MS results and quantitative UV-Vis titration, indicating that a majority of EDTA remains under these three

forms in solution. This allows estimating EDTA speciation all along the diffusion experiment (Figure 3). The speciation of EDTA is only slightly modified during 200 days (80 % of [Ca/Mg-Na-EDTA]⁻), and evolves to a majority of iron species after 400 days (almost 95 % of [Fe^{III}-EDTA]⁻). This result is confirmed by Fe measurments performed by atomic absorption experiments and also presented in Figure 3. The concentration of Fe^{3+} in solution rises to a plateau with a value close to EDTA concentration. It was not possible to quantify the amount of both oxidation states Fe^{+II} or Fe^{+III} in the diluted samples. The importance of iron release by such perturbation is discussed further in section 4.2.
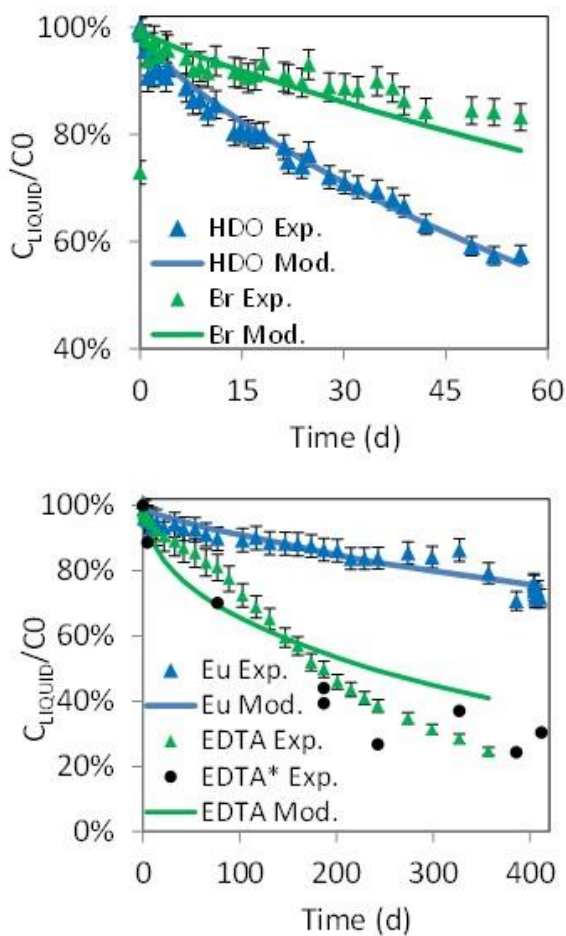

Figure 2. Experimental and modelled concentrations in solution (Exp. / Mod.). Top : HDO and Br. Bottom: EDTA and Eu. EDTA* results obtained by ESI-MS (S^{TOT}).
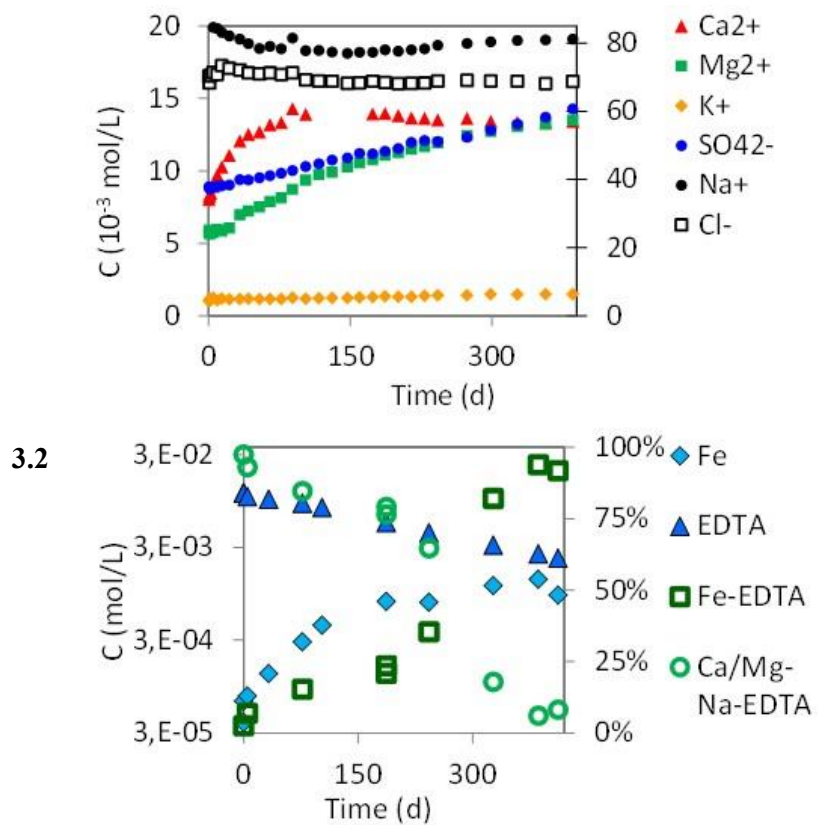
Figure 3. (Top) Concentration of ions in solution. (Na+ and Cl- on the right ordinate). (Bottom) Speciation of EDTA. Left ordinate, Fe and EDTA concentrations. (Right ordinate) Speciation of EDTA in solution extrapolated from ESI-MS data.

11

Solid profiles

The diffusion profiles measured by leaching of the solid samples are presented in figure 4. Five profiles are available for HDO and Br$^-$. In both cases, the tracers penetrate deeper in the Y direction, parallel to the rock bedding, than in the Z axis, normal to the bedding, indicating a diffusion anisotropy. The concentrations of Br at the extremity of profiles (Y, Z > 10 cm) are close to zero and in the order of magnitude of the detection limit. Two profiles were obtained for EDTA. In the case of europium, four profiles were acquired from leached samples and one with the total concentration obtained by total mineralization of the solid. Adjustments of transport parameters and discussion are presented in the next section.
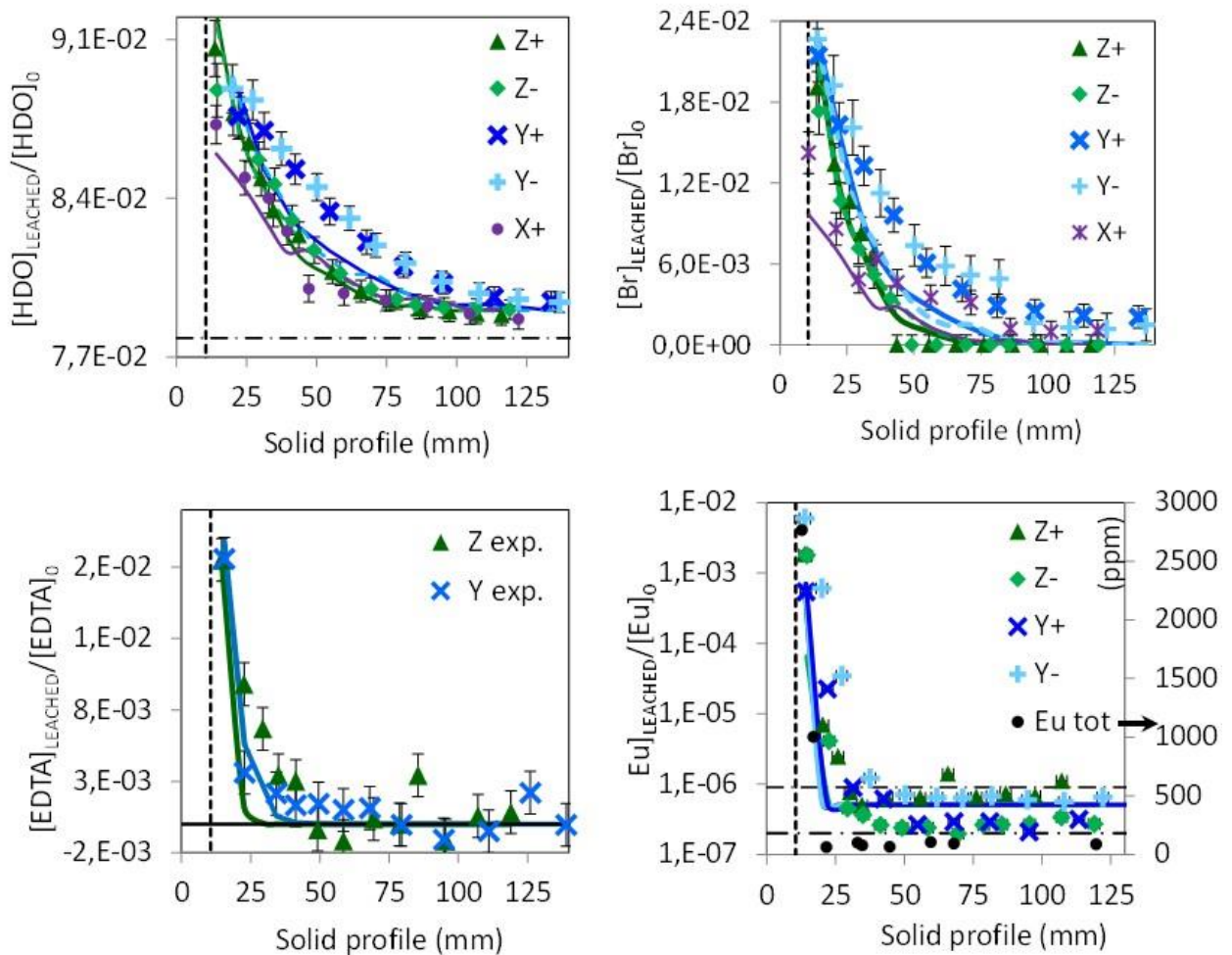

Figure 4. Concentration of HDO, Br, EDTA and Eu tracers in the solid profiles.

Data are normalized by the initial concentration in the liquid, [C]liq.(t=0).

Solid curves represent best fitting.

4. Modelling and discussion

4.1 HDO and Br- transport parameters and diffusion anisotropy

The modelling of the HDO and bromide diffusion is compared to experimental results in figures 2 (liquid profile) and 4 (solid profiles). Results from the parametric adjustment performed on these curves with (De, R, a) as parameters are gathered in table 2. In the case of HDO, another parameter k<1 was adjusted, replacing $\epsilon_a \times m/\rho$ by $k \times \epsilon_a \times m/\rho$ in equation (3) in order to take into account evaporation during the solid cutting. $D_e(HDO)$ and $\epsilon_a(HDO)$ values are consistent with transport parameters obtained by through-diffusion experiments on small samples of the same depth (Descostes et al., 2008). The diffusion of HDO along XY axis, $D^{\parallel} = a \times D_e = 4.5 \ 10^{-11} \ m^2 \ s^{-1}$ is also close to values obtained by Samper et al. (2008) on similar large scale sample $(4.0 \ 10^{-11} \ m^2 \ s^{-1} < D^{\parallel}(HTO) < 4.51 \ 10^{-11} \ m^2 \ s^{-1})$, which is described as the most accurate parameter obtained by the author. The value of anisotropy, a(HTO) = 1.65 [1.6-1.8], is also close to the value a(HTO) = 1.79 obtained by Samper et al. (2008). In the case of bromide, an anionic exclusion is observed with low transport parameters, $D_e(Br)/De(HDO)=[30-50\%]$ and $\epsilon_a(Br)/\epsilon_a(HDO)=[46-75\%]$. These data are slightly higher to data measured by through-diffusion on small COx samples: $D_e(Cl)/De(HTO)=[11-21\%]$; $\epsilon_a(Cl)/\epsilon_a(HTO)=[33-53\%]$; $D_e(I)/ \ D_e(HTO)=[7-26\%]$ (Descostes et al., 2008; Savoye et al., 2012a). It is noteworthy that HDO and Br were injected 400 days after EDTA, and diffuse in the perturbed zone of the clay rock.
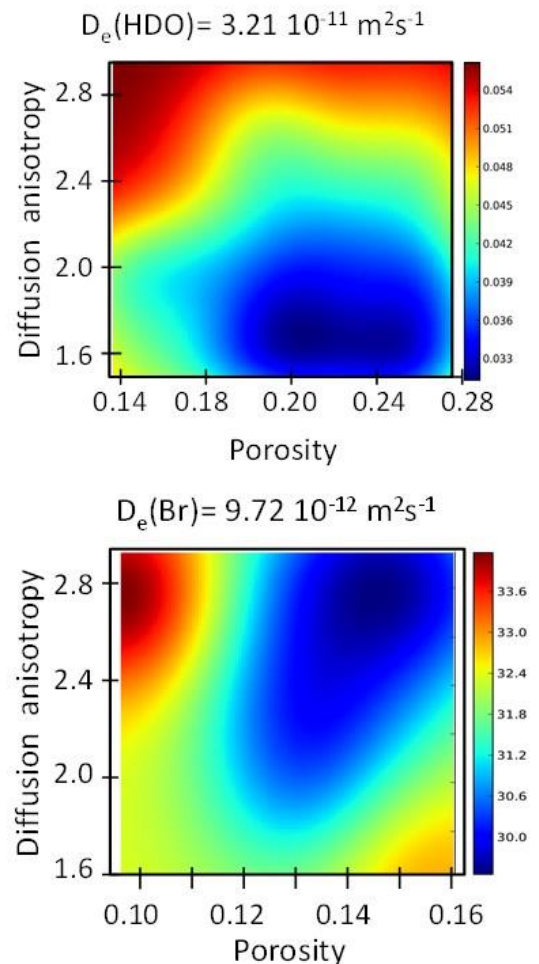

Figure 5. Minimization criterion for HDO (Top) and Br (Bottom) as a function of accessible porosity, εa, and diffusion anisotropy, a = De $\parallel$(X,Y) / De⊥(Z).

All these results indicate a limited effect of the 10 mM organic plume on the porosity of the rock and on anions transport.

Knowing diffusion anisotropy of anions with accuracy is crucial to estimate the release of radionuclides. Few data are available on non-perturbed clay rock samples. Cormenzana et al. (2008) performed measurements on a large-scale COx sample (a(HTO) = 1.5-3.2). Samper et al. (2008) performed further analysis of these data, giving an optimum value: a(HTO)=1.79. They also evidenced a limited accuracy on the anisotropy factor (1.79 < a(HTO) < 3.8). Similar values were obtained on Boom clay (a(HTO, I⁻)~2 and a=1.4 for organic matter) whereas much higher values were evidenced for Opalinus clay: a ~ 5.1 / 3.8 / 2.6 for HTO, I, and Br respectively (Gimmi et al., 2014). Still, large-scale experiments seem to be necessary to confirm results from in situ experiments. Indeed, the geological formations are sensitive to anisotropic regional stress, leading to extensional and shear fractures close to boreholes (Vinsot et al., 2014). These fractures may potentially affect the estimation of diffusion anisotropy. In our case, the size of the injection chamber and the long-term rehydration suggests a self-sealing of the rock. The values and accuracy on ε_a(HDO/Br) and a(HDO/Br) are illustrated in Figure 5, which report the minimization criterion as a function of these parameters. Relatively low anisotropies were obtained (a(HDO) = 1.65 and a(Br⁻) = 2.75), indicating a limited effect of the perturbation. All these data and ranges are gathered in table 2.

4.2 Transport and behaviour of EDTA

Since EDTA complexes are mainly under anionic form, further modelling were performed with $\varepsilon_a = 0.144$ and a = 2.75 taken from bromide results. Strikingly, it was not possible to adjust both liquid monitoring and solid profile for EDTA results, using only (D_e, α) as parameters. We did not use a specific adsorption law for EDTA since the adsorption isotherm measured on COx clay is almost linear from 10^{-7} up to 10^{-2} mol L⁻¹ (Dagnelie et al., 2014). The best fit obtained with two parameters (D_e, α) displays a large underestimation of the decrease of the liquid concentration. This result suggested that desorption of EDTA during the leaching step is not complete and that adsorption of

EDTA is partially irreversible or kinetically blocked. Such behaviour was observed in various systems, especially for amino acids on sedimentary rocks (Liu and Lee, 2007).

Species	$D_e^\perp$ $(10^{-12}\ m^2\ s^{-1})$	a $= D^\parallel/D^\perp$	α $= R\ \varepsilon$	K_d $(L\ kg^{-1})$	References
HDO	**32.1** **[29-36]**	**1.65** **[1.6-1.8]**	$\varepsilon^{HDO} = 0.21$ **[20-26]**		**This work**
HTO	[8-15] 22.3 [12-26]	[2.5-3] 1.79 [1.79-3.8]	$\varepsilon^{HTO} = 0.16$ $\varepsilon^{HTO} = 0.16$		[1] [2]
Br⁻	**9.7** **[8-13]**	**2.75** **[2.4-2.9]**	$\varepsilon^{Br-} = 0.14$ **[0.12-0.15]**		**This work**
Cl⁻	4.4-8.9		$\varepsilon^{Cl-} = 0.08 \pm 0.02$		[3]
EDTA	**3.9**		$\alpha = 9.0\ \varepsilon_a = \varepsilon^{Br}$	**3.8 (In-Diff)** **0.089 (Leach.)**	**This work**
	0.94		$\alpha = 0.27$ (Cell) with $\varepsilon_a = \varepsilon^{Cl}$	6.2 (Batch) 0.08 (Cell)	[4]
Eu^{III}- EDTA	**0.17**		$\alpha = 13.5$ with $\varepsilon_a = \varepsilon^{Br}$	**5.8 (In-Diff)** **0.16 (Leach.)**	**This work**
Eu^{III}- EDTA	0.5-1.3		2.5 - 6.3	3.4-16 (Batch) 0.56-1.2 (Cell)	[5]

Table 2. Diffusion parameters obtained in COx clay rock. Values between brackets represent the uncertainty ranges. References : [1] Cormenzana et al. 2008, [2] Samper et al. 2008, [3] Garcia-Gutierrez et al. 2008, [4] Dagnelie et al. 2014, [5] Dagnelie et al. 2012.

To get a quantitative estimation of the desorption hysteresis, we performed a three parameters adjustment: (D_e, α, K_d*). $K_d=[(\alpha - \varepsilon_a)]/[\rho \times (1-\varepsilon_a)]$, estimated from adjusted parameter α, represents the total adsorption during the diffusion experiment. K_d*, used in equation (3) instead of K_d, represents the reversible fraction of ETDA desorbed during leaching. Figures 2 and 4 show the corresponding best fits obtained with 3 parameters. The model still doesn't fit the exact shape of the liquid monitoring. An

inflection point is observed on the liquid monitoring curve at t = 100 days, probably linked to the rearrangement of the initial speciation due to dissolution and release of calcium and iron. This result indicates that Ca/Mg-Na-EDTA and Fe-EDTA species may have rather different transport parameters and require additional experiments to be discriminated with accuracy. Thus, one should use carefully the EDTA parameters gathered in Table 2. These adjusted parameters should primarily be dedicated to physical interpretation of the perturbation. The values for K_d and K_d* are 3.8 L kg^{-1} and 0.089 L kg^{-1} respectively. These are still consistent with values previously obtained on COx samples by through-diffusion experiment, with $K_d \sim 6.2$ L kg^{-1} measured by batch experiment and $K_d \sim 0.08$ L kg^{-1} measured by through-diffusion (Dagnelie et al., 2014). The adsorption value (K_d) is more likely representative of total capacity of adsorption, as measured in batch or in-diffusion experiment. K_d*, which was introduced because of the desorption hysteresis, gives only a qualitative estimation of the reversible fraction of diffusing species.

The slow dissolution of iron-rich phases increases the concentration of Fe into the liquid chamber, inducing a modification of EDTA speciation (Figure 3). It is to note that such a phenomenon was not observed in previous through-diffusion experiments performed with ^{14}C-EDTA or [152]Eu-EDTA, even with longer contact time between solution and COx clay rock (> 600 days, Dagnelie et al., 2012). This discrepancy can be related to the lower volume / mass ratio (V/m(Diffusion-cell) $\sim$ 17.7 L kg^{-1}) compared to the ratio used in this study (V/m(Large-scale) $\sim$ 4 10^{-3} L kg^{-1}). Kinetics of dissolution processes were already studied on various mineral phases: for example, on iron oxides (Noren et al., 2009) and hydroxides (Nowack and Sigg, 1997), calcite and magnesite (Pokrovsky et al., 2009), Mg-Zn-Ferrite (Keny et al., 2006). It is noteworthy for simulations at longer time scale that the release of iron in solution under Fe-EDTA form could also catalyze the degradation of EDTA which is usually stable in solution in absence of heat, bacterial activity or radiation (Means et al., 1980; Metsärinne et al., 2001). Some preliminary tests were performed by X-ray diffraction and no alteration was evidenced on the major clay-rich phases (data not shown). Thus, released iron seems to originate from minor phases such as pyrite or Fe-(hydr)oxides dissolution. This hypothesis needs to be confirmed and further experiments will be necessary to determine which minor phase(s) are dissolved, which species are released (Al, Si, Fe), and what are the corresponding kinetics. Such data

are relevant for two reasons. Firstly hydrous iron oxides are known to affect organics adsorption (Saidy et al., 2013). Secondly, cations released by minor phases will potentially compete with radionuclides, modifying adsorption or complexation. For example, dissolution of iron in geological or engineered barriers could limit the available stock of complexing molecules which are considered as penalizing in term of radionuclides confinement.

4.3 Transport and behaviour of EDTA-Eu^{III}

The europium profiles obtained by leaching or by mineralization (Figure 4) show similar trends. The decrease of europium concentration in the rock is sharper ($\sim$ 20 mm) than for EDTA ($\sim$ 40 mm) indicating a low effective diffusion coefficient but also a adsorption of Eu^{III} reduced by EDTA complexation. As for EDTA, it was not possible to adjust simultaneously liquid monitoring and solid profiles of Eu-EDTA with only two parameters. The best fit obtained with three parameters (De, α, Kd*) is given in figures 2 and 4 and corresponding values are presented in table 2. The value of the effective diffusion, D_e(Eu-EDTA) $\sim$ 0.25 10^{-12} m^2 s^{-1}, is close to transport parameters measured for organic complexes by through-diffusion experiments indicating an anionic exclusion of the negatively charged complex [Eu-EDTA]$^-$ as discussed previously. The adjustment of parameter α leads to a K$_d$ value of 5.8 L kg^{-1}, which confirms the low but significant adsorption of the EDTA complex, regardless of the linked cation (Ca^{II}, Fe^{III} or Eu^{III}). The lower value of the third parameter (K$_d$* $\sim$ 0.16 L kg^{-1}) indicates that [Eu-EDTA] also displays a adsorption hysteresis during the leaching step, as well as other EDTA complexes. In order to determine transport parameters of the EDTA complexes with accuracy, a complete reactive-transport model will be necessary. It should include dissolution rates, complexation in solution as well as a better understanding on desorption hysteresis.

Conclusion

A diffusion experiment was performed on large-scale COx clay rock sample with a perturbation induced by a 10 mM EDTA plume. The liquid to solid ratio of the experiment was $V/m \sim 4 \cdot 10^{-3}$ L kg^{-1} close to environmental or in situ conditions in soils remediation and nuclear waste storage. Transport of HDO, Br^{-}, EDTA, and Eu^{III} was monitored from the liquid injection chamber through the rock during 450 days. Three transport parameters could be adjusted by use of both liquid monitoring and post-mortem solid profiles: effective diffusion perpendicular to the bedding of the rock (D_e), accessible porosity (ε_a), and diffusion anisotropy (a). Transport parameters of HDO are close to small scale experiments ($D_e^{\perp}$(HDO) $\sim 3.2 \cdot 10^{-11}$ m^2 s^{-1}, $\varepsilon^{HDO} \sim 0.21$, a(HDO)=1.65). Values for bromide indicate an anionic exclusion in the COx clay (D_e(Br)/D_e(HDO) ~ 0.3-0.5, ε_a(Br)/ε_a(HDO) ~ 0.67). The diffusion anisotropy for anion was adjusted to 2.75 and varies in the range [2.4-2.9], depending on accuracy on ε_a. All these results indicate a limited effect of the perturbation on the porosity and properties of the rock.

The negatively charged EDTA complexes, including [Fe-EDTA]$^{-}$ and [Eu-EDTA]$^{-}$, are significantly adsorbed by COx. A desorption hysteresis is observed for both organic complexes. This behaviour limits the standard model from reproducing all experimental results. The adjusted parameter K_d(EDTA/Eu-EDTA) $\sim 3.8/5.8$ L kg^{-1} is in the same range than previous observations made on batch experiments. [Ca/Mg-Na-EDTA] complexes and [Eu-EDTA]$^{-}$ display low apparent diffusion coefficient through COx clay rock, $D_e/\alpha \sim 4.3 \cdot 10^{-13}$ m^2 s^{-1}, and $1.3 \cdot 10^{-14}$ m^2 s^{-1} respectively. All these transport parameters must be used cautiously since they are obtained within a perturbed state of the rock.

Despite a limited effect of the perturbation, a fast dissolution of carbonates is observed until a new equilibrium is reached between calcite and solution. Then a slow dissolution of minor phases (iron-rich) is also evidenced, followed by a retro-diffusion of Fe in the liquid system. The knowledge of the kinetics and solid phase(s) dissolved in presence of AOM will be necessary to complete a reactive-transport modelling. Furthermore, the release of cations from minor phases under perturbation

may be important because it modifies the complexing capacity of organic molecules, potentially limiting (or enhancing) their effect on metal or radionuclides migration.

References

Alonso, U., Missana, T., Garcia-Gutierrez, M., Patelli, A., Albarran, N., Rigato, V., 2011. Colloid diffusion coefficients in compacted and consolidated clay barriers: Compaction density and colloid size effects. Physics and Chemistry of the Earth, Parts A/B/C 36, 1700-1707.

Andra, 2014. GL transfert, Rapport de synthèse 2007-2014. Technical report, CG.RP.ASTR.14.0013.

Bryan, N.D., Abrahamsen, L., Evans, N., Warwick, P., Buckau, G., Weng, L., Riemsdijk, W.H.V., 2012. The effects of humic substances on the transport of radionuclides: Recent improvements in the prediction of behaviour and the understanding of mechanisms. Applied geochemistry, 27, 378-389.

Churchman, G.J., Gates, W.P., Theng, B.K.G., Yuan, G., 2006. Chapter 11.1 Clays and Clay Minerals for Pollution Control, Developments in Clay Science, 1, 625-975.

Cormenzana, J., Garcia-Gutierrez, M., Missana, T., Alonso, U., 2008. Modelling large-scale laboratory HTO and strontium diffusion experiments in Mont Terri and Bure clay rocks. Physics and Chemistry of the Earth, Parts A/B/C 33, 949-956.

Dagnelie, R., Descostes, M., Radwan, J., Blin, V., 2012, Migration de complexes organiques dans l'argile du Callovo-Oxfordien: synthèse du cas Eu-EDTA, Congrès Tranfert 2012, Ecole Centrale de Lille, 20-21-22 mars 2012.

Dagnelie, R., Descostes, M., Pointeau, I., Klein, J., Grenut, B., Radwan, J., Lebeau, D., Georgin, D., Giffaut, E., 2014, Sorption and diffusion of organic acids through clayrock: comparison with inorganic anions. Journal of Hydrology, 511, 619-627.

Darban, A.K., Foriero, A., & Yong, R.N., 2000. Concentration effects of EDTA and chloride on the retention of trace metals in clays. Engineering Geology, 57(1–2), 81–94.

Descostes, M., Blin, V., Bazer-Bachi, F., Meier, P., Grenut, B., Radwan, J., Schlegel, M.L., Buschaert, S., Coelho, D., Tevissen, E., 2008. Diffusion of anionic species in Callovo-Oxfordian argillites and Oxfordian limestones (Meuse/Haute-Marne, France). Applied Geochemistry 23, 655-677.

Drever, J.I., Stillings, L.L., 1997. The role of organic acids in mineral weathering. Colloids and Surfaces A: Physicochemical and Engineering Aspects 120, 167-181.

Durce, D., Landesman, C., Grambow, B., Ribet, S., Giffaut, E., 2014. Adsorption and transport of polymaleic acid on Callovo-Oxfordian clay stone: Batch and transport experiments. Journal of Contaminant Hydrology, 164, 308-322.

Garcia-Gutierrez, M., Cormenzana, J., Missana, T., Mingarro, M., Alonso, U., Samper, J., Yang, Q., Yi, S., 2008. Diffusion experiments in Callovo-Oxfordian clay from the Meuse/Haute-Marne URL, France. Experimental setup and data analyses. Physics and Chemistry of the Earth, Parts A/B/C 33, S125-S130.

Gaucher, E., Robelin, C., Matray, J., Négrel, G., Gros, Y., Heitz, J., Vinsot, A., Rebours, H., Cassagnabère, A., Bouchet, A., 2004. ANDRA underground research laboratory: interpretation of the mineralogical and geochemical data acquired in the Callovian–Oxfordian formation by investigative drilling. Physics and Chemistry of the Earth, Parts A/B/C 29, 55-77.

Gimmi, T., Leupin, O.X., Eikenberg, J., Glaus, M.A., Van Loon, L.R., Waber, H.N., Waber, H.N., Wersin, P., Wang, A.O., Grolimund, Borca, N., Dewonck, S., Wittebroodt, C. 2014. Anisotropic diffusion at the field scale in a 4-year multi-tracer diffusion and retention experiment – I: Insights from the experimental data. Geochimica et Cosmochimica Acta, 125, 373–393.

Guggenberger, G., Kaiser, K., 2003. Dissolved organic matter in soil: challenging the paradigm of sorptive preservation. Geoderma 113, 293-310.

Harter, R.D., Naidu, R., 1995. Role of Metal-Organic complexation in metal sorption by soils, Advances in Agronomy, 55, 219-263.

Keny, S.J., Manjanna, J., Venkateswaran, G., Kameswaran, R., 2006. Dissolution behavior of synthetic Mg/Zn-ferrite corrosion products in EDTA and NTA based formulations. Corrosion Science 48, 2780-2798.

Lee, S.Y., Tank, R.W., 1985, Role of clays in the disposal of nuclear waste: A review, Applied clay science, 1, 1-2, 15-162.

Liu, Z., Lee, C., 2007. The role of organic matter in the sorption capacity of marine sediments. Marine Chemistry 105, 240-257.

Maes, N., Bruggeman, C., Govaerts, J., Martens, E., Salah, S., Van Gompel, M., 2011. A consistent phenomenological model for natural organic matter linked migration of Tc(IV), Cm(III), Np(IV), Pu(III/IV) and Pa(V) in the Boom Clay. Physics and Chemistry of the Earth, Parts A/B/C 36, 1590-1599.

Martens, E., Maes, N., Weetjens, E., Van Gompel M., Van Ravestyn, 2009. Modelling of a large-scale in-situ migration experiment with 14C-labelled natural organic matter in Boom Clay, Radiochimica Acta, 98, 695–701.

Means, L., J.L., Kucak, T., Crerar, D.A., 1980. Relative degradation rates of NTA, EDTA and DTPA and environmental implications. Environmental Pollution Series B, Chemical and Physical 1, 45-60.

Melkior, T., Yahiaoui, S., Thoby, D., Motellier, S., Barthes, V., 2007. Diffusion coefficients of alkaline cations in Bure mudrock. Physics and Chemistry of the Earth, Parts A/B/C 32, 453-462.

Metsärinne, S., Tuhkanen, T., Aksela, R., 2001. Photodegradation of ethylenediaminetetraacetic acid (EDTA) and ethylenediamine disuccinic acid (EDDS) within natural UV radiation range. Chemosphere 45, 949-55.

Montarnal, P., Mugler, C., Colin, J., Descostes, M., Dimier, a, Jacquot, E., 2007. Presentation and use of a reactive transport code in porous media. Physics and Chemistry of the Earth, Parts A/B/C 32, 507-517.

Nagy, N.M., Kónya, J., Wazelischen-Kun, G., 1999. The adsorption and desorption of carrier-free radioactive isotopes on clay minerals and Hungarian soils. Colloids and Surfaces A: Physicochemical

and Engineering Aspects 152, 245-250.

Nogueira, F., Lopes, J., Silva, a, Goncalves, M., Anastacio, a, Sapag, K., Oliveira, L., 2009. Reactive adsorption of methylene blue on montmorillonite via an ESI-MS study. Applied Clay Science 43, 190-195.

Noren, K., Loring, J.S., Bargar, J.R., Persson, P., 2009. Adsorption Mechanisms of EDTA at the Water-Iron Oxide Interface : Implications for Dissolution. Journal of Physical Chemistry C 113, 7762-7771.

Nowack, B., Sigg, L., 1997. Dissolution of Fe(III) (hydr)oxides by metal-EDTA complexes. Geochimica et Cosmochimica Acta, 61, 5, 951-963.

Parkhurst, D.L., 1995. User's guide to PHREEQC: a computer program for speciation, reaction path, advective transport, and inverse geochemical calculations. USGS Water resources investigations report, 95–4227.

Pociecha, M., Lestan, D., 2012. Novel EDTA and process water recycling method after soil washing of multi-metal contaminated soil. Journal of hazardous materials 201-202, 273-9.

Pignatello, J.J. 1999. The Measurement and Interpretation of Sorption and Desorption Rates for Organic Compounds in Soil Media. Advances in Agronomy, 69, 1-73.

Poinssot, C., Geckeis, H., 2012. Radionuclide behaviour in the natural environment. Woodhead Pub LTD. Chapter 5, Reiller, P.E., Buckau, G., Impacts of humic substances on the geochemical behaviour of radionuclides, 103-160. Chapter 12, van Loon, L., Glaus, M., Ferry, C., Latrille, C., Studying radionuclide migration on different scales: the complementary roles of laboratory and in situ experiments, 446-483.

Pokhrel, D., Viraraghavan, T., 2004. Treatment of pulp and paper mill wastewater--a review. The Science of the total environment 333, 37-58.

Pokrovsky, O.S., Golubev, S.V., Jordan, G., 2009. Effect of organic and inorganic ligands on calcite and magnesite dissolution rates at 60 ° C and 30 atm pCO2. Chemical Geology 265, 33-43.

Reiller, P.E., 2012. Modelling metal–humic substances–surface systems: reasons for success, failure and possible routes for peace of mind. Mineralogical Magazine, 76, 7, 2643–2658.

Reinoso-maset, E., Worsfold, P.J., Keith-roach, M.J., 2012. The effect of EDTA, NTA and picolinic acid on Th(IV) mobility in a ternary system with natural sand. Environmental Pollution 162, 399-405.

Saidy, A.R., Smernik, R.J., Baldock, J.Aa., Kaiser, K., Sanderman, J. 2013. The sorption of organic carbon onto differing clay minerals in the presence and absence of hydrous iron oxide. Geoderma, 209-210, 15–21.

Samper, J., Yang, Q., Yi, S., García-Gutiérrez, M., Missana, T., Mingarro, M., Alonso, Ú., Cormenzana, J.L., 2008. Numerical modeling of large-scale solid-source diffusion experiments in Callovo-Oxfordian clay. Physics and Chemistry of the Earth, Parts A/B/C 33, S208-S215.

Sarazin, G., Michard, G., Prevot, F., 1999. Technical note. A rapid and accurate spectroscopic method for alkalinity measurements in sea water. Water Research 33, 290-294.

Savoye, S., Frasca, B., Grenut, B., Fayette, A., 2012a. How mobile is iodide in the Callovo-Oxfordian claystones under experimental conditions close to the in situ ones? Journal of contaminant hydrology 142-143C, 82-92.

Savoye, S., Michelot, J.-L., Matray, J.-M., Wittebroodt, C., Mifsud, A., 2012b. A laboratory experiment for determining both the hydraulic and diffusive properties and the initial pore-water composition of an argillaceous rock sample: a test with the Opalinus clay (Mont Terri, Switzerland). Journal of contaminant hydrology 128, 47-57.

Seliman, A.F., Borai, E.H., Lasheen, Y.F., Abo-Aly, M.M., DeVol, T.A, Powell, B.A., 2010. Mobility of radionuclides in soil/groundwater systems: comparing the influence of EDTA and four of its degradation products. Environmental pollution (Barking, Essex : 1987) 158, 3077-84.

Uzumasa, Y., Nishimura, M., Seo, T., 1956. Ultraviolet Spectrophotometric Determination of iron with Ethylenediaminetetraacetic Acid. Bulletin of the Chemical Society of Japan 30, 438-442.

Vinsot, A., Leveau, F., Bouchet, A., Arnould, A., 2014. Oxidation front and oxygen transfer in the fractured zone surrounding the Meuse/Haute-Marne URL drifts in the Callovian–Oxfordian argillaceous rock. Geological Society, London, Special Publications, 400.